

COMPUTATIONAL FLUID DYNAMICS SIMULATION OF THE ATUCHA II NUCLEAR POWER PLANT REACTOR

Damian Ramajo, Santiago Corzo, Santiago Márquez Damián and Norberto Nigro

*International Center for Computational Methods in Engineering (CIMEC)
INTEC-UNL-CONICET, Güemes 3450 S3000GLN Santa Fe, Argentina
dramajo@santafe-conicet.gov.ar*

Keywords: CFD, PHWR, flow and thermal distribution

Abstract. A Computational Fluid Dynamics (CFD) simulation of the Heavy Water Pressure Reactor (PHWR) of the Atucha II nuclear power plant was developed. A 3-dimensional (3D) detailed model was employed to simulate the upper and lower plenums, the down comer and the hot-legs and cold-legs. The control rods and the coolant channel walls were also included to account for their influence on flow mixing. The behavior of the coolant channels was modeled by imposing the nominal mass flow at mass and momentum sinks and sources at the location of the inlet and outlet coolant channel ports, respectively. The hydraulic zone distribution was also considered, applying different mass flow rates according to the local coolant channel location. In this preliminary work, the nominal mass flow rate was imposed to the channels to know the steady state reactor behavior. Latterly the mass flow rate through each one of the coolant channels was calculated based on the local pressure at the channel ends at the lower and upper plenums. Simulations allowed a deep understanding of the complex thermo-hydraulic phenomena inside the reactor plenums. The temperature profile and the velocity field inside the upper plenum could be visualized. This computational model is the first step for developing a real time dynamic model, which will be capable to simulate unsteady conditions and some typical operational problems like control rod stepping caused by thermal stratification in the hot-legs or hot-leg streaming.

1 INTRODUCTION

The Nuclear Power Plant Atucha II (*CNA II*) have a pressurized heavy water reactor (*PHWR*) with a total thermal power of 2160 MWt and a electric power of 745 MWe. The reactor pressure vessel (*RPV*) is a vertical core configuration with 451 coolant channels (*CC*) arranged in a 272 mm trigonal lattice pitch within the moderator tank. Each *CC* contents a bundle of 37 natural uranium (UO_2) fuel rods of 5300 mm active length. Fuel bundles consist of fuel rods arranged in three concentric circles, the rod supporting plate, the spacers for lining up the fuel rods, and the linkage with a coupling for connection to the filler machine. During reactor operation the fuel bundles are continuously removed from the *CCs* by the refueling machine in order to control the reactivity and the fuel burnup and to replace the exhausted fuel. That means that the reactor does not need to stop for refueling.

CCs are cooled by heavy water (D_2O). The reactor is also moderated by D_2O . The heat generated in the fuel assemblies is transferred to the coolant, which flows confined inside the *CCs*, transporting the heat to two steam generators. *CCs* are surrounded by the moderator, which is enclosed in the moderator tank. For reactivity reasons, the moderator is maintained at a lower temperature than the coolant. The heat extracted to the moderator is employed for pre-heating the light water that feed the steam generators.

There are two coolant loops and four moderator loops. The reactor coolant system and the moderator system are connected by the pressure equalization openings of the moderator tank closure head. Therefore, the pressure differences in the core are comparatively small. For control of the reactivity the reactor contains nine hafnium and nine steel control rods. In addition to the rod control, the reactor have a boric acid dosing system. The injection or extraction of boric acid serves to compensate slow reactivity changes due to the burnup during the first period of operation and to maintain the reactor in a safe subcritical condition at zero power. The reactivity can also be controlled by varying the moderator temperature (*FSAR chapter IV, 2011*). *Table 1* consigns some general characteristics and nominal operation conditions of the *RPV*.

Property	Inlet	Outlet
Heavy water (D_2O)		
Mass flow rate	10576 kg/s	10576 kg/s
Temperature	277.8 °C	314.6 °C
Saturation temperature	320.5 °C	
Density		
Viscosity		
Pressure	115 bar	107.7 bar
Reactor Pressure Vessel (<i>RPV</i>)		
Total thermal power	2160 MWt UO_2	
Total electric power	746 MW	
Maximum channel power	6.863 MW*	
Total number of hot channels	451	
Number of fuel rods for fuel assembly	37	
Number of control rods	18	

*Corresponding to *CC* 147.

Table 1: General characteristics and nominal operation conditions of the *RPV*.

A view of the *RPV* cutting one hot-leg and one cold-leg is showed in *Figure 1*. The scratched solids above the upper and below the lower plenums are the filler bodies, which serve to reduce the volume of the coolant in the reactor coolant system.

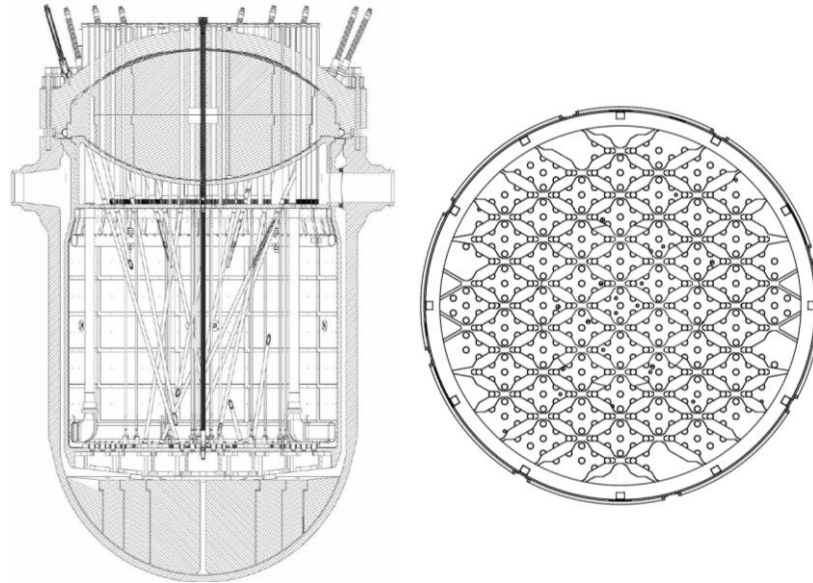


Figure 1: Left: cross sectional cut of the *RPV*. Right: sketch of the rhomboidal flow distributor at the lower plenum and the location of the *CCs*

The *RPV* constitutes the pressure boundary of the reactor core, enclosing the core components and the *RPV* internals. The *RPV* consists of the lower part, the closure head and the studs and nuts which connect both sections. The technology of *CNA II* and its predecessor Atucha I (*CNA I*) was discontinued around the 80`s and any other similar nuclear power plant was constructed around the world. Although the experience gained with *CNA I*, *CNA II* is two times larger than the first, getting a challenge, especially for simulation.

Regarding the flow circuit, the *RPV* can be divided in the lower and upper plenums, the down comer, the moderator tank and the coolant channels. The coolant enters to the *RPV* through two cold legs (one of the nozzles is showed at the left side in Figure 1 at the left) and downs to the lower plenum through the annular down comer. The lower plenum have a rhomboidal flow distributor, in which the *CCs* are grouped in subgroups of 9 *CCs* as maximum (see Figure 1 at the right). The coolant enters to the *CCs* and flow ups towards the upper plenum, extracting heat from the fuel bundles.

For reactivity reasons, the *CC* are grouped in five hydraulic zones. Based on the local power of the *CC*, in each zone the nominal mass flow rate (*MFR*) is limited by means of flow restrictors (except for the zone 5) placed at the *CC* inlets. The zone 5 is the most important, containing 253 of the 451 *CCs* and around 70% of the total coolant *MFR*. Table 2 summarizes the principal characteristics of the five hydraulic zones. Note that the channel power limit increases almost three times from the zone 1 to the zone 5. A similar ratio is observed for the *MFR*.

Property	Hydraulic zone				
	1	2	3	4	5
Total number of hot channels	30	36	42	90	253
Maximum channel power (MW)*	2.239	2.992	3.959	5.442	6.863
Minimum channel power (MW)*	1.908	2.640	3.641	5.442	6.343
Average channel power (MW)*	2.052	2.812	3.837	5.268	6.661
Channel power limit (MW)	2.524	3.158	4.036	5.565	7.062

*Estimated by simulation (Courtesy of NASA)

Table 2: Characteristics of the five hydraulic zones.

The open literature reports several papers regarding pressure drop studies in specific reactor components. The majority is devoted to characterize the fuel bundles (Le Corre et al, 2010; Krepper et al, 2007; Vijayan et al, 1999; Anglart et al, 1997; Kurul and Podowsky, 1991). Correlations for predicting the pressure drop can be found in literature for typical spacer grids (Anglart et al, 1997; Brennen, 2005; Ghiaasiaan, 2008). As for reactor simulation, papers are frequently based on pilot plant reactors and almost exclusively modeling the reactors using 0/1 dimensional simulators (Hainoun et al, 2010; Bokhari and Mahommood, 2005; Hainoun et al, 1996). although, some papers concern to real power plant reactors applying *CFD* tools (Chiang et al., 2010; Chatzikriakou et al, 2010; Chi-Thanh and Truc-Nam, 2009).

2 COMPUTATIONAL MODEL

A cut view of a half of the computational model of the *RPV* is showed in Figure 2. A novel strategy for *CC* modeling considering the upper and lower ends as sink/source points (*SSP*) was implemented. In the upper plenum, the hot legs, twenty two control and measurement rods, the four vertical moderator inlets and the two elbow moderator outlets were considered. Besides, vertical cylinders (red cylinders) were placed above each one of the fifty nine *SSPs*. As for the lower plenum, the two cold legs, the down comer and the rhomboidal flow distributor were included. In the computational model the upper and lower plenums are two isolated domains joined through the *SSPs* which transport mass from one domain to the other. The heat transferred from the fuel rods to the coolant was represented by an enthalpy increment imposed over the coolant temperature.

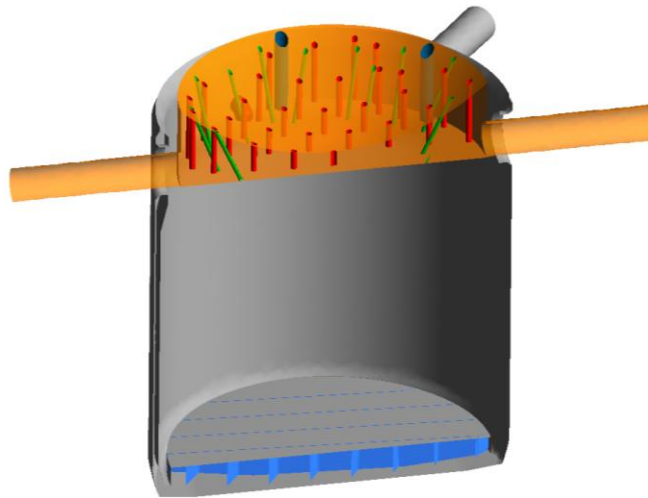


Figure 2: View of a half of the *RPV* geometry

In this preliminary work two simulations were performed; one for light water and the other for heavy water. For light water the data base IAPWS IF97, which is extensively used and allowed in CFX-13 (ANSYS-CFX 2010), was employed. Since for heavy water data for the reactor conditions was not available, the IAPWS IF97 for light water was also employed, but reducing the reactor temperature in order to obtain higher density and viscosity conditions (around 11% for density and 25% for viscosity).

The *SSP* methodology for representing the coolant channels was implemented in CFX-13 by using point sources. At run time simulation each point call to a *user function* for calculating the *MFR*, the temperature and the vertical velocity of the flow. All the *user*

functions are associated to a unique User Fortran Routine (*UFR*), which receives the current flow conditions (pressure and temperature) of each *SSP* and calculates the requested variables. [Figure 3](#) shows the points representing the sinks and sources of the *SSPs* located at the lower and upper coolant-channel ends, respectively. A preliminary model with fifty nine *SSPs* was used to represent the whole 451 *CC*. Each lower point of the *SSPs* was located inside of one rhomboidal cell of the lower plenum flow distributor which houses the coolant channel inlets. The *MFR* associated to each *SSP* was the sum of the *MFR* of the *CCs* located in the corresponding cell. For the case of distributor cells containing nine *CCs*, the *SSP* was placed at the central *CC*, while for those distributor cells containing less than nine *CCs* the *SSP* was located at the position of the *CC* with the highest *MFR*.

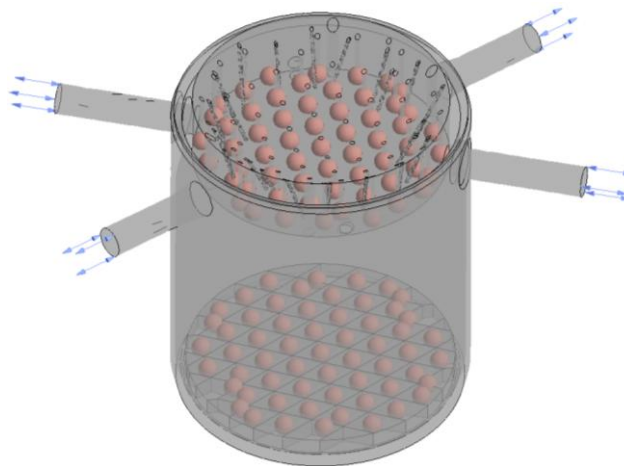


Figure 3: Computational model of the *RPV* showing the *SSP* locations

Although the currently implemented model has real time capability for a rough estimation of the *MFR* by a linear function of the pressure difference (ΔP_{ssp}) between the upper and the lower points of the *SSP*, a more real function for *MFR* vs. ΔP_{ssp} was not yet implemented in the *UFR*. Initial simulations using a linear function for *MFR* vs. ΔP_{ssp} allow to find some instability problems related to strong pressure fluctuations around the *SSPs* that directly impacted on the *MFR*. For this reason, in this preliminary work it was decided to impose the expected *MFR* for each *SSP*.

The computational domain was discretized with a mesh of 5.536.522 elements and 1.188.389 nodes. A local refinement by means of prism extrusion was applied at the walls. [Figure 4](#) shows some views displaying the local refinement.

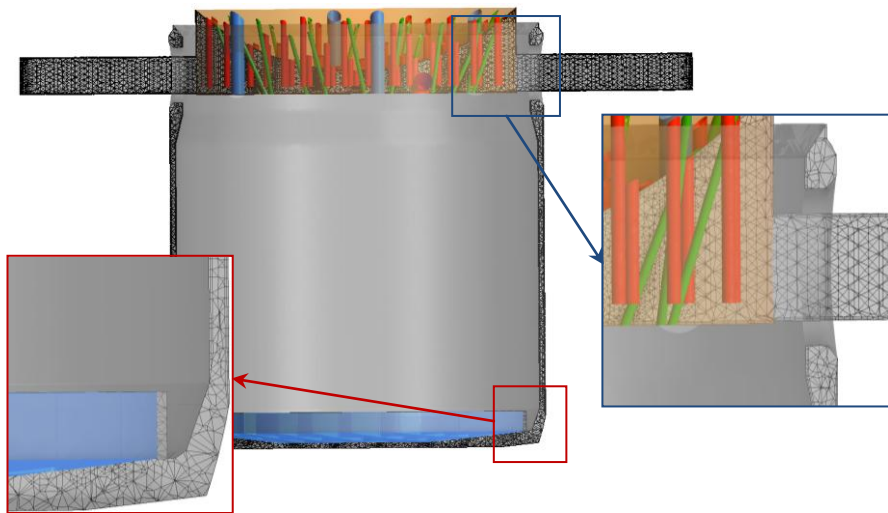


Figure 4: Views displaying the inner mesh of the RPV

3 GOVERNING EQUATIONS

The single-phase Navier-Stokes equations of mass, momentum and energy implemented in the finite volume commercial software ANSYS-CFX 13 were employed for simulations. The continuity equation is:

$$\frac{\partial \rho}{\partial t} + \nabla \cdot (\rho U) = 0 \quad (1)$$

where ρ is the density and U the velocity. Regarding the momentum equation, it can be written as:

$$\frac{\partial}{\partial t} (\rho U) + \nabla \cdot (\rho U U) = -\nabla P + \nabla \cdot \bar{\tau} + \rho \vec{g} \quad (2)$$

where P is the static pressure and τ is the shear stress tensor. Energy balance is accomplished by:

$$\frac{\partial}{\partial t} (\rho h_{tot}) - \frac{\partial P}{\partial t} + \nabla \cdot (\rho U h_{tot}) = \nabla \cdot (\lambda \nabla T) + \nabla \cdot (U \tau) \quad (3)$$

where h_{tot} is the total enthalpy, calculated from the static enthalpy by:

$$h_{tot} = h + \frac{1}{2} U^2 \quad (4)$$

In Eq. 3 λ is the heat transfer coefficient and the term $\nabla \cdot (U \tau)$ is the work associated to viscous stresses.

The standard two equation k - ε model was employed to model turbulence and a standard logarithmic wall law was applied to represent the logarithmic velocity profile near walls, thus avoiding high mesh refinement (ANSYS-CFX Theory guide, 2010). k - ε model has been extensively employed to simulate multiphase systems due to its robustness and accuracy even with relatively rough meshes. The transport equations for the turbulent kinetic energy k and the turbulence dissipation rate ε are:

$$\frac{\partial(\rho k)}{\partial t} + \frac{\partial(\rho U k)}{\partial x_j} = \frac{\partial}{\partial x_j} \left(\frac{\mu_t}{\sigma_k} \frac{\partial k}{\partial x_j} \right) + G_t - \rho \varepsilon \quad \text{with } j=1,2,3 \quad (5)$$

$$\frac{\partial(\rho \varepsilon)}{\partial t} + \frac{\partial(\rho U \varepsilon)}{\partial x_j} = \frac{\partial}{\partial x_j} \left(\frac{\mu_t}{\sigma_\varepsilon} \frac{\partial \varepsilon}{\partial x_j} \right) + \frac{\varepsilon}{k} (C_1 G_t - C_2 \rho \varepsilon) \quad \text{with } j=1,2,3$$

where μ_t is the turbulent viscosity, which is obtained from the eddy viscosity model,

$$\mu_t = \frac{C_\mu \rho k^2}{\varepsilon} \quad (6)$$

C_1 , C_2 , σ_k , σ_ε and C_μ are model constants, being 1.44, 1.92, 1.0, 1.3 and 0.09, respectively. In Eq. 5 and 6, G_t is a turbulence production term estimated from the velocity gradient and the turbulent viscosity μ_t as:

$$G_t = \frac{1}{2} \mu_t \left(\nabla u^2 + (\nabla u)^T \right)^2 \quad (7)$$

Regarding time integration, a first order Backward Euler scheme was applied. A range of pseudo-time steps from 1×10^{-3} s. to 1×10^{-4} s. were studied. *RMS* residual for mass and momentum were quite larger around 5×10^{-4} while for the energy was 5×10^{-6} and for turbulence were less than 1×10^{-4} . The mass balance at the upper and lower domains was carefully controlled. It was noted that a non typical relationship between the pseudo-time step and the mass balance was verified, requiring no to reduce but increase the time step up to 5×10^{-3} sec. in order to obtain discrepancies less than 1% between *RPV* inlet and outlet. Equations were solved using local parallel computing facilities in a Intel(R) Core(TM) i7 CPU 950 3.07 GHz, 6 GB RAM.

3.1 Boundary conditions and initialization

Although in steady-state normal operation the flow enters to the *RPV* through the cold legs and leaves it through the hot legs, opening conditions were imposed for both boundaries.

Steady simulations imposing the nominal MFR at the channels showed no convergence problems even for pseudo-time steps higher than 5×10^{-3} sec. Although, the nominal pressure at the inlet was set from the beginning and steady-state was reached after less than 200 iterations.

3.2 Coolant channel pressure drop

The single-phase pressure drop depending on friction, contraction or expansion effects can be calculated using the following equation:

$$\Delta P = \sum_{i=1}^n \xi_i \frac{G_i^2}{2\rho} \quad (8)$$

where ΔP is the pressure drop, ξ_i is the pressure drop coefficient and G is the local mass velocity. In general ξ_i are a function of the geometry as well as the Reynolds number (Re). The friction coefficient (f) in straight tubes for turbulent flow can be determined using the Lehmann correlation (Chapter IV-FSAR, 2010):

$$f^{-0.5} = 1.94 \log \left\{ \left[\left(\frac{4.26}{Re} \right) f^{-0.5} \right]^{1.1} + \left[\frac{1}{3.71} \left(\frac{e}{D_H} \right) \right]^{1.03} \right\}, \quad \text{with } D_H = \frac{4A}{s} \quad (9)$$

where e is the roughness, s is the wetted perimeter and A the cross transversal area. Then, the pressure drop coefficient associated to frictional efforts is:

$$\xi_{ff} = f \frac{l}{D_H} \quad (10)$$

where l is the duct length. The local pressure drop caused by the presence of inlet throttle restrictors can be estimated by the following correlation:

$$\Delta P = \xi_o \left(\frac{Re}{Re_o} \right)^b \quad (11)$$

where ξ_o and b are constants experimentally obtained (Camps, 1992) and Re_o is a reference Re . In this correlation the constants were calculated by assuming a hydraulic diameter equal to the inner diameter of the CC .

4 RESULTS AND DISCUSSION

Preliminary results corresponding to nominal steady state conditions are presented. Results are basically oriented to describe the overall flow behavior and evaluate the potentiality of the computational model using SSP s for CC modeling.

4.1 Flow distribution at nominal conditions

The flow distribution at the expected nominal conditions, that is imposing the MFR and temperature at the SSP s, were simulated in order to know the theoretical or expected flow behavior at the upper and the lower plenums. Clearly, this kind of simulation can be carried out without the SSP coupling strategy, but the information about the ΔP_{ssp} from the simulations was then used to estimate the corresponding MFR applying Eq. 8, thus allowing comparison with the imposed ones. Simulations were performed both for light and heavy water, comparing the pressure drop along the down comer and lower plenum.

Figure 6 shows the flow velocity over some horizontal and vertical planes cutting the RPV . Note that velocities at the hot and cold legs are higher than 10 m/s and similar velocities are reached around the locations of the upper points of the SSP s. In reality, the coolant velocity at the CC upper throttles is considerably smaller [Corzo et al, 2011], but the fact that each SSP groups several CC s led to a locally higher MFR .

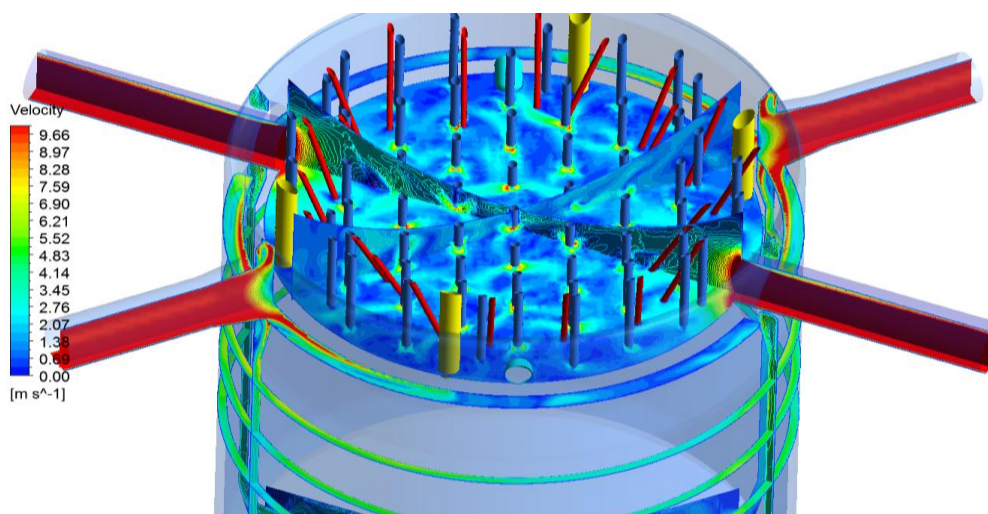


Figure 6: Flow velocity over vertical and horizontal cutting planes

Figure 7 shows the velocity pattern over a vertical plane cutting the cold legs. Although the joint between the cold legs and the *down comer* have a divergent shape the flow detaches from the inner wall impacting the moderator tank wall and descending close to it. The flow inside the upper plenum is very complex even considering that only 59 of the 451 coolant channel walls were included. Inside the down comer annulus the flow is not completely homogeneous and the velocity ranges from 1 to 5 m/s. All the rhomboidal cells of the flow distributor of the lower plenum show vortex flow structures of the size of the cell. Velocities are quite higher and the central *SSPs* corresponding to the higher *MFR* induce velocities up to 2 m/s in all cells.

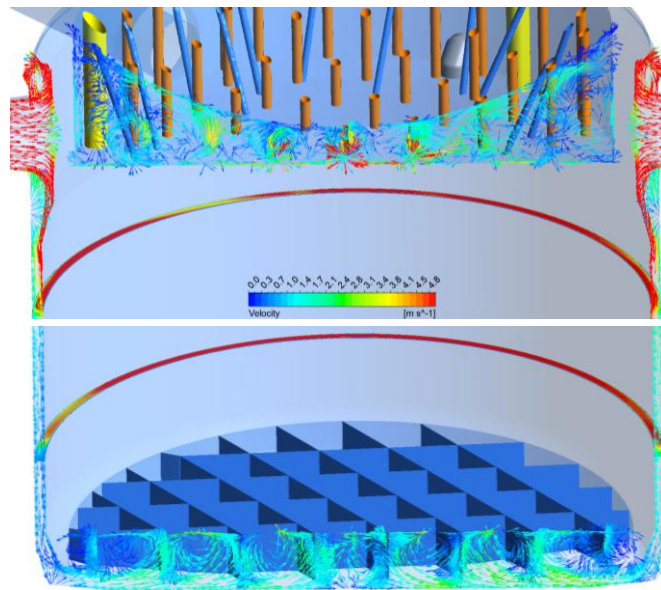


Figure 7: Velocity pattern over a vertical plane cutting the cold legs

Figure 8 at the left shows streamlines of the flow entering the *RPV* and descending through the down comer. Note that flow quickly is distributed at the whole annulus. This behavior can also be appreciated by analyzing the velocity over the two horizontal planes cutting the down comer at Figure 7. Figure 8 at the right shows the streamlines starting from the *SSPs* at the upper plenum. Note that flow follows the shorter way to reach the hot legs.

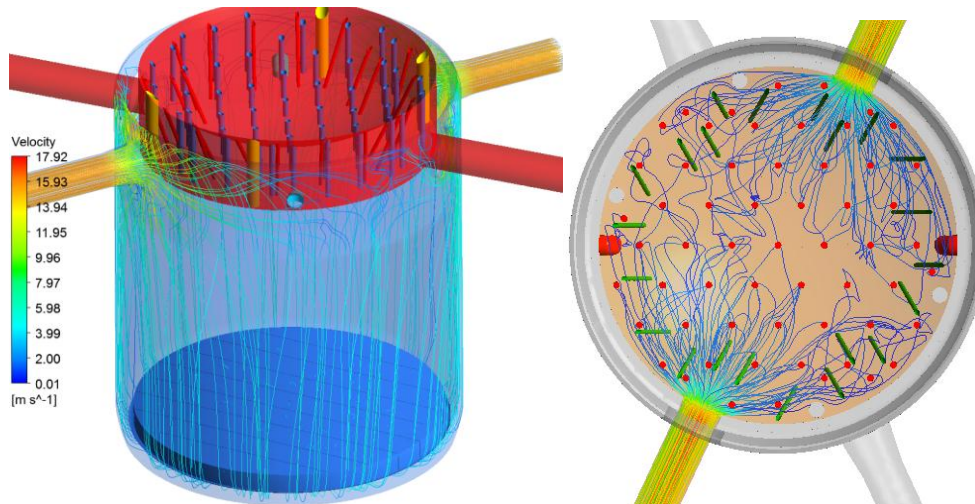


Figure 8: Streamlines showing the flow distribution at the down comer annulus (left) and inside the upper plenum (right)

Figure 9 allows to visualize the velocity pattern over a vertical plane cutting the hot legs. Note that flow is strong accelerated around the outlet ducts. Mixing is very intense in part due to the control rods and *SSPs* walls but mainly due to the velocity of the flow injected. The inlet and outlet moderator tank duct seems not have a significant effect on the flow maybe due to the fact that the strongly motion is located at the central zone.

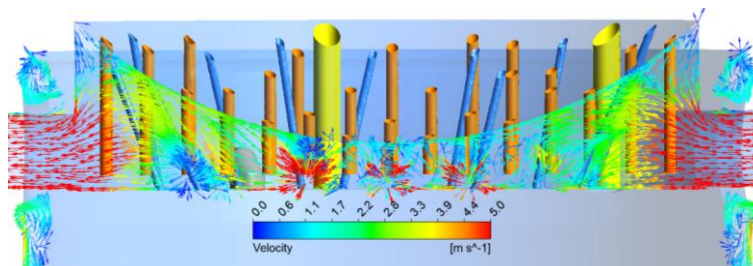


Figure 9: Velocity pattern over a vertical plane cutting the hot legs

Figure 10 shows the temperature profile over a vertical plane cutting the hot legs. Note that although the *RPV* walls were set as adiabatic the slightly difference on temperature was due to the temperature of the coolant injected from the hydraulic zone 5 was 0.2°C higher than the rest. In future work the radial power distribution of the *RPV* will be incorporated in order to visualize and quantify thermal stratification in the hot-legs or hot-leg streaming.

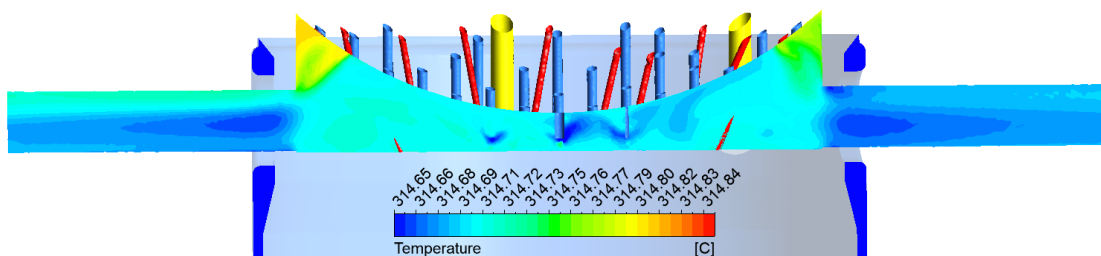


Figure 10: Temperature profile over a vertical plane cutting the hot legs

4.2 Pressure drop through the reactor

The pressure drop through the different reactor zones was estimated by comparing the area average total pressure at four cross transversal planes (planes *PH1* to *PH4*) at the down comer annulus and two ring surfaces (*SR1* and *SR2*) at the lower plenum. Figure 11 shows the ΔP from the *RPV* inlet to the lower plenum. The main ΔP is located at the joint between the cold legs and the annulus. Then, the ΔP at the annulus is smaller and the lower plenum shows almost the same total pressure for the two ring surfaces. Note that ΔP is smaller for the heavy water than for the light one.

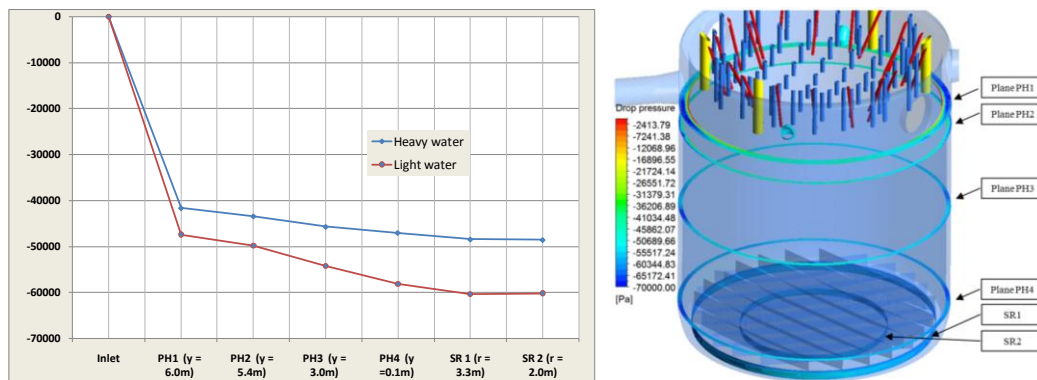


Figure 11: Pressure drop from the inlet to the lower plenum

4.3 Pressure drop and MFR through the coolant channels

CFD data previously obtained for the real geometry of the *CC* (Corzo et al, 2011) allowed to find a function relating the *MFR* and the ΔP along the *CC* for each hydraulic zone. *CC* were assumed as the sum of locally concentrated (also named form losses) and long distributed or frictional pressure drop. For the first group the main important are: the thirteen spacers, the outlet port throttle at the upper end and the inlet flow restrictor at the bottom end. For the second group, the frictional losses are basically located at the thirty seven fuel rods and the channel wall. The frictional loss at the spacer walls are significant, but they are included in the local loss coefficient of the spacer.

From *CFD* (Corzo et al, 2011) the pressure drop coefficient ξ for the upper throttle was 1.86. As for spacers, the corresponding ξ ranged from 0.951 to 0.908 for $2.5 \times 10^5 < Re < 5.8 \times 10^5$. Finally, ξ for the inlet restrictors was experimentally obtained (FSAR chapter IV, 2010; Camps, 1992). Table 3 summarizes the pressure drop coefficients ξ_i .

Application of Eq. 8 along with the coefficients from Table 3 allowed to estimate the ΔP at each hydraulic zone for heavy and light water (see Table 4). Note that the ΔP along the *CC* progressively decreases from the hydraulic zone 1 to the 5. Excepting for the unthrottled zone, the largest ΔP are caused for the presence of the flow restrictors.

CC component	Pressure drop coefficient
Inlet flow restrictor*	
Hydraulic zone 1	ξ_0 : 867.1 b:-0.014
Hydraulic zone 2	ξ_0 :520.8 b:-0.046
Hydraulic zone 3	ξ_0 :276.8 b:-0.065
Hydraulic zone 4	ξ_0 :79.3 b:-0.032
Hydraulic zone 5	ξ_0 :1.09 b:0.0
Spacers	ξ : 0.951 to 0.908 ($2.5 \times 10^5 < Re < 5.8 \times 10^5$) *
Outlet throttle	ξ : 1.32
Fuel rod + channel wall	C_f : 0.0185, 0.0182, 0.0179, 0.0176, 0.0175 ξ : 8.066, 7.932, 7.812, 7.686, 7.613

* Corresponding to one spacer

Table 3: Pressure drop coefficients ξ_i for the different CC components.

	Coolant channel pressure drop [bar]*				
	Hydraulic zone				
	1	2	3	4	5
Nominal <i>MFR</i>	9.29	11.70	15.08	21.27	27.73
ΔP restrictor	5.956 5.383	5.325 4.847	4.462 4.079	2.699 2.449	0.068 0.062
ΔP spacers	0.391 0.356	0.613 0.559	1.001 0.916	1.957 1.774	3.292 2.989
ΔP frictional	0.255 0.234	0.398 0.364	0.650 0.594	1.271 1.157	2.139 1.943
ΔP throttle	0.059 0.053	0.093 0.084	0.154 0.139	0.307 0.277	0.522 0.470
ΔP total	6.661 6.026	6.429 5.854	6.267 5.726	6.232 5.657	6.021 5.464

* Considering fluid properties at the average pressure and temperature (\bar{P} =111.35 bar, \bar{T} =296.5°C)

Table 4: Pressure drop ΔP along the coolant channels for light (grey) and heavy (black) water.

As was mentioned, in this preliminary model of the RPV the *MFR* at the *SSPs* were constrained in order to visualize the expected or nominal flow scenario. But, although the *MFR* is imposed, the static pressure at the inlets and the outlets of the *SSPs* was monitored and results were used to estimate the corresponding *MFR* under these pressure differences by iteratively apply the Eq. 8. It is clear that, for a more real estimation of the *MFR* a real-time iterative simulation must be done. Figure 12 at the left shows the imposed (blue line) and the estimated (green line) *MFR*. Note that for the firsts thirty *SSPs* estimation are far from the expected. Looking at the ΔP_{ssp} (see Figure 12 at the right) the upper pressure seems to be larger than the required. That can be explained by the fact that the contraction of 9 CC in one *SSP* causes unrealistic local pressure grown, reducing the pressure difference ΔP_{ssp} . Besides, it was observed that the position of the upper points of some *SSPs* have significant incidence on the local pressure at these points. On the other hand, all these factors are minimized for the *SSPs* with the smaller *MFR* (from 40 to 59) for which good agreement is found. Figure 13 allows to visualize the later, note that the pressure at the lower point of the *SSPs* have scarce variation while the pressure at the upper points ranged from 111 bar for the central *SSPs* to 109 bar for the periphery ones.

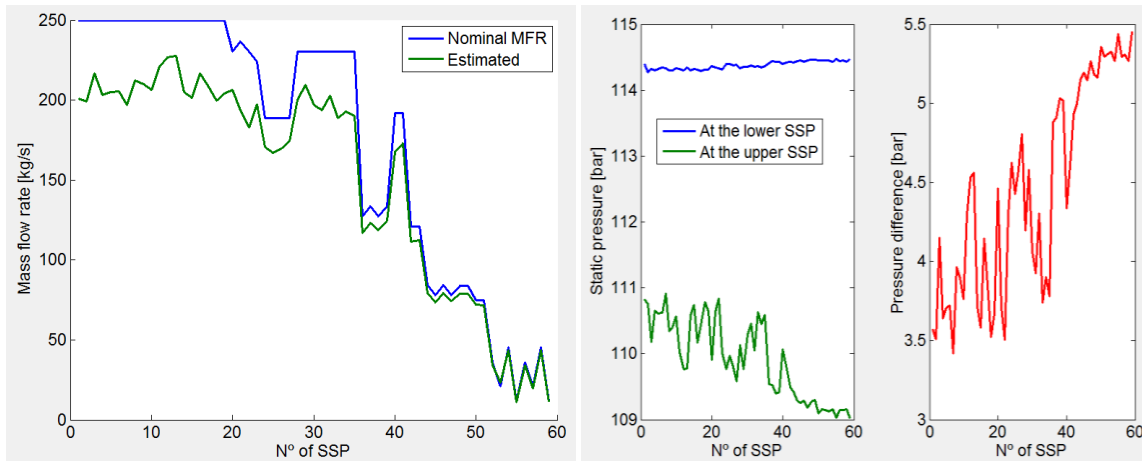


Figure 12: Heavy water results. Left: imposed and estimated MFR at the *SSP*. Right: static pressure at the lower and upper points and ΔP_{ssp} of the *SSPs*

5 CONCLUSION AND FUTURE WORK

The present work is a first step for developing a more complex and more realistic *RPV* computational model. Results are preliminary but at the same time precursors by the fact that the strategy of using *SSPs* opens the possibility of modeling the overall *RPV*, which will be impossible without the implementation of a simplified model for the *CC*. This kind of strategy had not been reported in the open literature yet.

The obtained results allowed to verify the smaller pressure drop expected at the down comer and the good performance of the flow distribution at the lower plenum. The behavior of the flow distributor at the lower plenum showed to be in agreement with the expected, that evidenced by the small variation on the static pressure at the lower points of the *SSPs*. Future work is oriented to implementation of a dynamic real-time estimation of the *MFR* at the *SSPs* and the introduction of the radial power distribution. The increment of the amount of *SSPs* in order to model each one of the 451 *CC* also will be implemented. A more ambitious challenge will be to model the *CCs* as one dimensional channels considering the axial power distribution in order to know the temperature profiles and estimates the boiling phenomenon at the upper end of the *CC*.

Glossary

<i>RPV</i> :	Reactor pressure vessel
ΔP_{ssp} :	Static pressure difference between the upper and the lower coolant channel ends
<i>CFD</i> :	Computational fluid dynamics
<i>MFR</i> :	Mass flow rate [kg/s]
<i>CC</i> :	Coolant channel
<i>SSP</i> :	Sink/Source Point
<i>UFR</i> :	User Fortran Routine
<i>N-S</i> :	Navier-Stokes equations
<i>U</i> :	Reynolds averaged velocity
<i>P</i> :	Fluid density
ε :	Turbulent eddy dissipation rate
<i>k</i> :	Turbulent kinetic energy
λ :	Heat transfer coefficient
<i>CNA</i>	Nuclear Power Plant Atucha II

II:

PHWR: Pressurized heavy water reactor

UO₂: Natural uranium

DO₂: Heavy water (deuterium)

Re: Reynolds number

μ_t : Turbulent eddy viscosity

G_i : Turbulence production term

G : Mass velocity

ξ_i : Pressure drop coefficient

ΔP : Pressure drop

f : Friction coefficient

e : Roughness

s : Wetted perimeter

A : Cross transversal area

D_H : Hydraulic diameter

l : Duct length

ξ_0, b : Model constant for pressure drop coefficient for the restrictors

Acknowledgements

Authors want to thanks to CONICET, Universidad Nacional del Litoral and ANPCyT (grants PICT 1645 BID (2008), CAI+D 65-333 (2009)). Also they are gratefully to thank to Autoridad Regulatoria Nuclear (ARN) and Society for Plant and Reactor Safety of Germany (GRS) for invaluable technical support.

References

ANSYS-CFX solver theory guide, 2010.

Anglart H., Nylund O., Kurul N., Podowski M.Z., CFD prediction of flow and phase distribution in fuel assemblies with spacers, *Nuclear Eng. Design*, 177:215-228, 1997.

Brennen C., Fundamentals of Multiphase Flows, Cambridge Univ. Press, 2005.

Bokhari I.H., Mahomood T., Analysis of loss of flow accident at Pakistan research reactor-1, *Annals of Nuclear Energy*, 32:1963-1968, 2005.

Camps A., Analysis of Fuel Bundle and Different Inlet Throttle Experimental Pressure Drop Measurements, CNEA, 1992.

Chatzikiyriakou D., Walker S.P., Hewitt G.F., The contribution of non-wetting droplets to direct cooling of the fuel during PWR post-LOCA reflood, *Nuclear Eng. and Design*, in press, 2010.

Chiang J., Pei B., Tsai F., Pressurized water reactor (PWR) hot-leg streaming. Part 1: Computational fluid dynamics (CFD) simulations, *Nuclear Eng. and Design*, in press, 2010.

Chi-Thanh T., Truc-Nam D., The effective convectivity model for simulation of melt pool heat transfer in a light water reactor pressure vessel lower head. Part II: Model assessment and application, *Progress in Nuclear Energy*, 51:860-971, 2009.

Corzo S., Ramajo D., Marquéz Damian S. and Nigro N., CFD Simulation inside a PHWR Coolant Channel of the Atucha II Nuclear Power Plant, enviado para su presentación en *ENIEF 2011*, Noviembre de 2011, Rosario, Argentina, 2011.

FSAR chapter IV, 2011, NASA.

Ghiaasiaan M., Two-Phase Flow, Boiling and Condensation, Cambridge Univ. Press, 2008.

- Hainoun A., Hicken E., Wolters J., Modelling of void formation in the subcooled boiling regime in the ATHLET code to simulate flow instability for research reactors, *Nuclear Eng. and Design*, 167:175-191, 1996.
- Hainoun A., Grazi N., Mansour Abdul-Moaiz B., safety analysis of the IAEA reference research reactor during loss of flow accident using the code MERSAT, *Nuclear Eng. and Design*, 240:1132-1138, 2010.
- Kurul N., Podowsky M., On the modeling of multidimensional effects in boiling channels, *ANS Proc. 27th National Heat Transfer Conference*, Minneapolis, MN, July 28-31, 1991.
- Krepper E., Koncar B., Egorov Y., CFD modeling of subcooled boiling-Concept, validation and application to fuel assembly design, *Nuclear Eng. and Design*, 237:716-731, 2007.
- Le Corre J.M., Yao S.C, Amon C., A mechanistic model of critical heat flux under subcooled flow boiling conditions for application to one-and three-dimensional computer codes, *Nuclear Eng. and Design*, 240:235-244, 2010.
- Vijayan P.K., Pilkhwal D.S., Saha D., Venkat Raj V., Experimental studies on the pressure drop across the various components of a PHWR fuel channel, *Exp. Thermal and Fluid Science*, 20:34-44, 1999.